Shear Banding in Mesoscopic Dusty Plasma Liquids

Chia-Ling Chan, Wei-Yen Woon, and Lin I

Department of Physics, National Central University, Chungli, Taiwan 32054, Republic of China

(Received 7 June 2004; published 24 November 2004)

We experimentally demonstrate shear banding and construct a microscopic dynamic picture of a sheared 2D mesoscopic dust Coulomb liquid at the kinetic level. Under the topological constraints from the discreteness and finite boundary, the nonlinear threshold-type response of motion to the local stress induced by thermal and external drives leads to shear thinning and the enhanced avalanche-type local topological transitions with stress relaxation in the form of clusters. It causes the formation of the outer shear bands in which the mean shear rate, the velocity fluctuations, and the structural rearrangement rate are all enhanced, and leaves a weakly perturbed center band. The typical size of the cooperative hopping vortex (about three interparticle distance) sets up a common length scale for the widths of the confinement induced layering and the shear band.

DOI: 10.1103/PhysRevLett.93.220602 PACS numbers: 05.40.–a, 52.27.Lw, 61.20.–p, 83.50.Ha

The behavior of ultrathin liquid confined in a mesoscopic gap is a fundamental problem in nanoscience and technology [1]. As the gap width goes down to the molecular scale, structure and transport properties deviate from the bulk liquid, under the effects of discreteness, finite boundary, and thermal fluctuation [1–8]. For instance, the formation of a layered structure from the boundary and the sluggish flow with large fluctuation and nonlinear mean velocity response to the external stress have been observed [1,3–8]. Nevertheless, the rheological measurements have been mainly limited to the macroscopic velocity and stress on the boundary because of the difficulty of direct microscopic measurement at the small molecular scale.

In contrast to the mean velocity profile with a uniform shear rate for a bulk Newtonian flow between two oppositely moving parallel plates [9], shear banding has been observed in sheared glassy materials such as foams, micelles, dense colloids, and dense granular systems. The sheared flow tends to separate into bands with different shear rates through local stress relaxation [10–13]. A cold mesoscopic liquid also exhibits similar disordered packing and slow dynamics under the topological constraints from the discreteness effect and the boundary confinement [8]. However, unlike the negligible temperature effect in the glassy system, the thermal agitation in liquid provides an additional source for *unfrozen* disordered packing and motion even in the absence of external stress. At low external stress, whether it exhibits shear banding or a profile with uniform shear rate and its microscopic picture are still interesting open issues.

A dusty plasma crystal and liquid formed by micrometer sized particles negatively charged ($\sim 10^4$ electrons per particle) and suspended in a low pressure gaseous discharge are inspiring Coulomb systems to mimic and understand the microstructure and dynamics at the kinetic level through direct video visualization[14]. The waves in 2D crystals and collective excitations in liquids are a few examples [15,16]. Generic behavior such as layering transition and slow dynamics similar to other numerical findings have been demonstrated experimentally in our mesoscopic shear-free 2D dust Coulomb liquid [6,8]. In this work, the thin liquid is further sheared along the two opposite boundaries. Through tracking each particle displacement and measuring the dynamics of the associated local structural rearrangement, we report the direct microscopic observation of shear banding and explore the microscopic origin.

Microscopically, in a cold 2D liquid as shown in Fig. 1, the particle mutual interaction tends to generate ordered triangular lattice-type domains with small amplitude position oscillations, which can be deteriorated and reorganized through stick-slip string- or vortex-type hopping induced by stochastic thermal kicks [8,16]. The boundary confinement suppresses transverse hopping and causes the

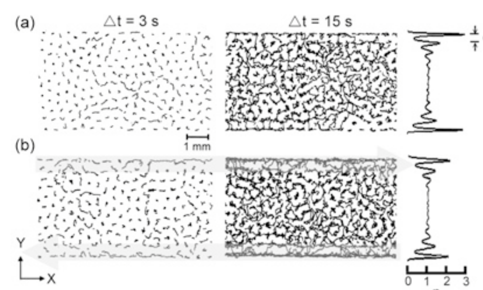

FIG. 1. (a) Typical particle trajectories with 3 and 15 sec exposure, and the transverse particle density distribution for the shear-free run showing the stick-slip hopping surrounding the temporarily ordered domain, and the confinement induced layering. (b) The corresponding figures for the shear run at 100 mW laser power. The gray arrows correspond to the position and the direction of the laser beams. The external stress enhances hopping, especially around the outer region, and reduces the oscillation amplitude of transverse density distribution.

formation of the nearby layered structure [Fig. 1(a)] [1,8]. The persistent and directional slow drive from the external stress along the boundary further enhances stick-slip-type structural rearrangements which cascade into the liquid through many-body interaction. In this study, we explore the regime where the external stress and thermal agitation have comparable strength. We find that the flow consists of two outer shear bands about three interparticle distance in width nearby boundaries and a center low rate zone. The former has higher levels of both longitudinal and transverse velocity fluctuations with skewed distribution. The shear banding phenomenon is originated from the local stress release through the avalanche-type local topological rearrangement events adjacent to the boundary.

In our experiment, a weakly ionized discharge ($n_e \sim 10^9\ \mathrm{cm}^{-3}$) is generated in 250 mTorr Ar gas using a 14 MHz rf power system operated at 2.0 W, similar to what described elsewhere [8]. The suspended and negatively charged polystyrene particles at 7 μm diameter are confined through the strong electric field in the surrounding dark space (sheath) adjacent to the two parallel vertical glass confining walls. Vertically, the suspended dust particles are aligned through the wakefield effect of the downward ion flow [17]. Particles in the same chain move together horizontally. The mean interchain distance a is 0.3 mm. This quasi-2D liquid has *smooth slipping boundaries.* Two parallel and counterpropagating cw laser sheets (488 nm Ar+ laser) with 0.4 mm half width and 2.5 mm height (covering the entire vertical chain) are introduced horizontally to push the two outermost rows of particles nearby each boundary. The radiation pressure is proportional to the laser power. The chain positions in the optical viewing plane are tracked digitally. The statistics are averaged over 10 000 picture frames. The averages are taken in strips 1 d in width and at different transverse distance Y from the boundary, where d (about 0.87 interparticle distance) is the interlayer spacing adjacent to the boundary (Fig. 1). The width of the liquid for the experiment is fixed at 10 d.

Figure 2(a) shows the nonlinear increase of the mean shear rate with the laser power (the thermal speed measured at a 10 sec interval is about 0.1 $d/$sec). The drop of the mean viscosity (shear rate divided by stress) with the increasing stress manifests shear thinning. Unlike the glassy material, no finite yield stress is found. Runs I, II, and III correspond to the shear-free run and the runs at 50 and 100 mW laser power, respectively. The mean longitudinal velocity profile measured at different Y [Fig. 2(b)] demonstrates the two outer high rate shear bands about 3 d in width sandwiching the center low rate zone. Increasing stress slightly increases the shear bandwidth. The particle trajectories and displacements in the shear bands exhibit larger fluctuations, which deteriorate the confinement induced layering [Fig. 1(b)]. Figure 2(c) shows the 20 sec longitudinal displacement histograms measured at different Y for runs I and III. For the shear-free run, the same distribution profiles illustrate the uniform longitudinal diffusion rate (the diffusion rate is proportional to the square of the variance). However, applying shear not only shifts the peak position but also broadens and skews the histograms in the shear band.

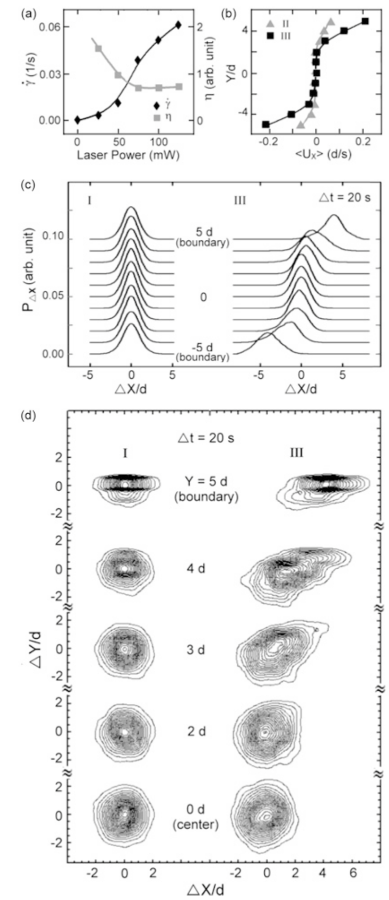

FIG. 2. (a) The nonlinear responses of the mean shear rate and viscosity to the laser power. Runs I, II, and III are the runs at 0, 50, and 100 mW, respectively. (b) The averaged longitudinal velocity profiles for runs II and III. Run I has zero mean velocity and is not plotted. (c),(d) The longitudinal displacement histograms and the contour plots of the 2D displacement histograms at different Y for runs I and III at 20 sec time intervals, respectively.

The 2D displacement histograms in Fig. 2(d) provide more detailed information. For the shear-free run, diffusion is highly anisotropic in the three outermost layers with suppressed transverse thermal motion by the boundary confinement [8]. Applying shear enhances both the longitudinal and the transverse fluctuations (diffusions) in the shear bands. The particles hopping outwards are exerted by larger longitudinal stress than those hopping inwards. It makes the displacement histograms skewed in the shear band. Note that the isotropic histogram in the center band ($|Y| \leq 2\ d$) is slightly broadened (variance increases 11%) and elongated when the stress enhanced hoppings are cascaded and randomized into the center zone.

The above shear banding phenomenon is strongly correlated to the local structural rearrangement, which can be characterized by tracking the temporal evolution of bond-orientational order (BOO) at each particle site **r**. BOO $= \Psi_6(\mathbf{r}) = |\Psi_6| \exp(i\theta_6) = \frac{1}{N_r}\sum_i \exp(i6\theta_k)$, where θ_k is the angle of the bond from the particle at r to its kth nearest neighbor, and N_r is the number of the nearest neighbors [16,18]. BOO is the Fourier transform of the angular distribution of the nearest neighbors for the $m = 6$ mode. θ_6 is the effective bond-orientation. $|\Psi_6| = 1$ and <0.4 for the perfect lattice site and the defect site with the nearest neighbor number deviating from 6, respectively [16]. Figure 3(a) shows the typical snapshots of the configurations of Ψ_6. The ordered domain (with large $|\Psi_6|$) is surrounded by defect clusters (with small $|\Psi_6|$) [19]. The subsequent change of Ψ_6 (i.e., $\Delta\Psi_6$) in 1 sec intervals [Fig. 3(b)] manifests the avalanche-type structural rearrangements in the form of clusters with large $\Delta\Psi_6$ through bond rotation, breaking, and reconnection, which are enhanced by applying the external stress. Figure 3(c) shows the temporal evolutions of $|\Psi_6|$ and the local bond angle θ_6 for typical particles sitting in the second outermost layers. The stronger high frequency oscillations evidences the faster stick-slip-type local stress accumulation and release through structural rearrangement after applying shear stress (note that the local stress and strain increase as $|\Psi_6|$ decreases [18]). The topological transitions alternately occur in different regions [19].

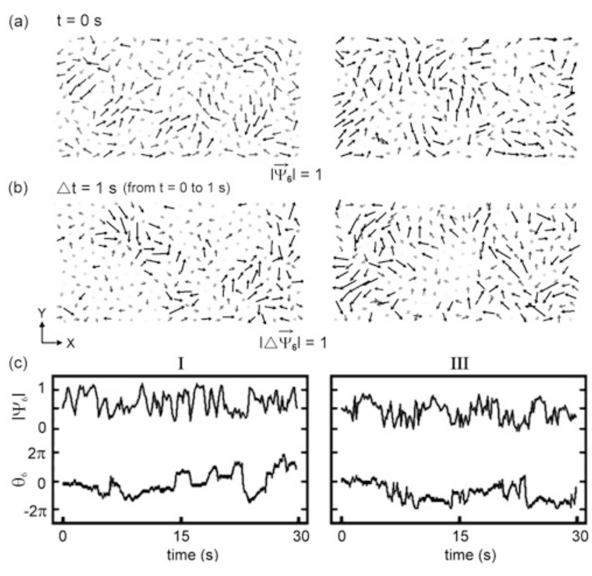

FIG. 3. Left column for run I and right column for run III. (a),(b) The typical snapshots of the spatial configurations of Ψ_6 and the subsequent change of Ψ_6 (i.e., $\Delta\Psi_6$) in 1 sec intervals, respectively. The orientation of Ψ_6 is θ_6. The length of Ψ_6 and $\Delta\Psi_6$ reflects the degree of local order and the structural change rate, respectively. (c) The typical stick-slip evolutions of the $|\Psi_6|$ and θ_6 for the typical particle at $Y = 3\ d$ (the third outermost layer).

The temporal correlations at different Y, $g_6(\tau) = \langle\Psi_6^*(\tau)\Psi_6(0)\rangle$, provide further statistical information. $g_6(0)$ $(= \langle\Psi_6^2\rangle)$ reflects the structural order. $g_6(\tau)$ decreases with time (about 1 sec correlation time) due to bond rotation of the ordered domain and hopping induced structural rearrangement [Fig. 4(a)]. Note that 1 sec is also the typical hopping time [16]. The slowest drop of $g_6(\tau)$ at the outermost layer [Fig. 3(a)] and the W shape transverse profile of $g_6(0)$ in Fig. 4(b) show the best structural order around the boundary due to confinement, and the worst structural order in the interface region 2 to 3 d from the boundary, to accommodate the different bond orientations between the outer layers and the temporarily ordered domains in the center zone. Applying external stress decreases both $g_6(0)$ and the correlation time at different Y. Figure 4(c) shows the Y dependence of the ratio R of the $g_6(\tau)$ of run III to that of run I. The R profile slightly deviates from one at $\tau = 0$ sec and then gradually drops with increasing τ to the W shape profile with the lowest value around the second and the third outermost layer ($|Y/d| = 2$ and 3) at $\tau = 2$ sec, where the reduction of the correlation time also reaches the maximum. It indicates that, even the structural order is only slightly decreased under external stress [also see Fig. 3(a)], the accumulation of the external stress induced motion with increasing time drastically speeds up the structural change rate in the shear band [also see Fig. 4(a) at $Y = 2\ d$]. In the center zone, it takes a longer time to accumulate the BOO change under the screened and randomized stress. The boundary alignment leaves the outermost layer least affected.

The above results provide a clear microscopic picture. In a cold liquid, particles are still densely packed with a

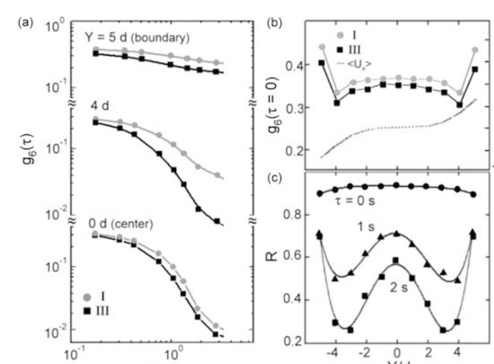

FIG. 4. (a) The temporal evolutions of $g_6(\tau)$ for the shear-free run I and the shear run III at different Y. (b) The Y dependences of $g_6(0)$ for runs I and III. The dotted curve shows the mean longitudinal velocity profile for run III as a reference for the location of the shear band. (c) The Y dependences of $R(\tau)$ at $\tau = 0$, 1, and 2 sec for the shear run III.

similar interparticle distance as solid. The mutual interaction tends to cage particle motion. It is the main source for slow dynamics. It sets up a threshold, only beyond which the accumulated local stress from thermal agitation or external drive can induce hopping and structural rearrangement. Consequently, shear thinning occurs. At the low stress limit, particles are still seriously affected by caging. Hopping is drastically enhanced as stress increases, which reduces the viscosity in the high stress regime.

Spatially, the external stress sets up a directional persistent drive along each boundary. Mediated through many-body interaction, the stress and hopping can be cascaded cooperatively through the neighboring particles into the disordered network and quickly randomized. Namely, the external drive induces local strain. The accumulated local stress is released through avalanche-type cooperative excitations of hopping and topological rearrangement involving a cluster of particles. The local regime is temporarily reformed to order until the next avalanche cycle. It leads to the enhanced longitudinal and transverse velocity fluctuations (diffusion) in the shear band. The stress relaxation and screening also leave a center region with low shear rate, because of shear thinning (high viscosity at the low stress end).

Regardless of the difference in the interaction forms and inertia, similar shear banding has also been observed in the glassy-type systems such as foams, micelles, granular systems, etc. [10–13], which have a negligible temperature effect. In particular, similar avalanche-type topological rearrangement involving clusters of a small number of particles have also been identified as the stress release process for the formation of shear banding in the foam system which has very low inertia [10]. The common microscopic physical origin can be traced back to the discreteness effect, which causes the caging from the topological constraints of neighboring particles and leads to the integrate-fire-type local stress release associated with topological rearrangement after accumulating sufficient strain energy. Inertia has a negligible effect because of the strong dissipation through the surrounding network. Note that the additional stochastic thermal agitation in our liquid system can promote as well as suppress the spatiotemporal cooperative excitation [16]. Unlike in the glassy system, jamming can be released by thermal kicks, which leads to the absence of a finite yield stress but a regime with high viscosity at the low stress end. The typical size (about 3 d) of the cooperative hopping vortex reflects the spatial correlation length of the bulk liquid at the microscopic level [8,16], which determines how far the boundary effects, such as confinement and external stress, on both structure and motion can be cascaded transversely into the system through the disordered network. Therefore, the widths of layered band induced by confinement and the shear bands share the common scale about 3 d [8].

This work is supported by the National Science Council of the Republic of China under Contract No. NSC92-0212-M008-042.

[1] For example, S. Granick, Phys. Today **52**, No. 7, 26 (1999).
[2] For example, J. Gollub, Phys. Today **56**, No. 1, 10 (2003).
[3] C. L. Rhykerd, Jr. *et al.*, Nature (London) **330**, 461 (1987).
[4] P. A. Thompson, G. S. Grest, and M. O. Robbins, Phys. Rev. Lett. **68**, 3448 (1992).
[5] M. Heuberger, M. Zach, and N. d. Spencer, Science **292**, 905 (2001).
[6] J. Gao, W. D. Luedtke, and U. Landman, Phys. Rev. Lett. **79**, 705 (1997).
[7] A. L. Demirel and S. Granick, Phys. Rev. Lett. **77**, 2261 (1996).
[8] L. W. Teng, P. S. Tu, and Lin I, Phys. Rev. Lett. **90**, 245004 (2003).
[9] For example, T. E. Faber, *Fluid Dynamics for Physicists* (Cambridge University Press, Cambridge, 1995).
[10] A. Kabla and G. Debregeas, Phys. Rev. Lett. **90**, 258303 (2003).
[11] J. B. Salmon, A. Colin, S. Manneville, and F. Molino, Phys. Rev. Lett. **90**, 228303 (2003).
[12] F. Varnik, L. Bocquet, J.-L. Barrat, and L. Berthier, Phys. Rev. Lett. **90**, 095702 (2003).
[13] Y. Jiang *et al.*, Phys. Rev. E **59**, 5819 (1999).
[14] J. H. Chu and Lin I, Phys. Rev. Lett. **72**, 4009 (1994); H. Thomas *et al.*, Phys. Rev. Lett. **73**, 652 (1994).
[15] J. B. Pieper and J. Goree, Phys. Rev. Lett. **77**, 3137 (1996); V. Nosenko, J. Goree, Z. W. Ma, and A. Piel, Phys. Rev. Lett. **88**, 135001 (2002).
[16] Y. J. Lai and Lin I, Phys. Rev. Lett. **89**, 155002 (2002).
[17] S. V. Vladimirov and M. Nambu, Phys. Rev. E **52**, R2172 (1995); S. V. Vladimirov and A. A. Samarian, Phys. Rev. E **65**, 046416 (2002).
[18] K. J. Strandburg, *Bond-Orientational Order in Condensed Matter Systems* (Springer, New York, 1992).
[19] W. Y. Woon and Lin I, Phys. Rev. Lett. **92**, 065003 (2004)